Foveated imaging for near-eye displays

GUANJUN TAN,[1] YUN-HAN LEE,[1] TAO ZHAN,[1] JILIN YANG,[2] SHENG LIU,[2] DONGFENG ZHAO,[2] AND SHIN-TSON WU[1,*]

[1]*College of Optics and Photonics, University of Central Florida, Orlando, Florida 32816, USA*
[2]*GoerTek Electronics, 5451 Great America Parkway, Suite 301, Santa Clara, CA 95054, USA*
[*]*swu@creol.ucf.edu*

Abstract: The angular resolution of current near-eye display devices is still far below human-eye acuity. How to achieve retina-level resolution while keeping wide field-of-view (FOV) remains a great challenge. In this work, we demonstrate a multi-resolution foveated display with two display panels and an optical combiner. The first display panel provides a wide FOV but relatively low resolution for the surrounding region, while the second one offers an ultra-high resolution for the central fovea region, by an optical minifying system which enhances the effective resolution by 5 ×. In addition, a switchable Pancharatnam-Berry phase deflector is employed to shift the high-resolution region. The proposed design effectively reduces the pixelation and screen-door effect in near-eye displays.

References and links

1. O. Cakmakci and J. P. Rolland, "Head-worn displays: A review," J. Disp. Technol. **2**(3), 199–216 (2006).
2. H. Hua, "Enabling focus cues in head-mounted displays," Proc. IEEE **105**(5), 805–824 (2017).
3. B. Bastani, E. Turner, C. Vieri, H. Jiang, B. Funt, and N. Balram, "Foveated pipeline for AR/VR head-mounted displays," Inf. Disp. **33**(6), 14–19 (2017).
4. C. Vieri, G. Lee, N. Balram, S. H. Jung, J. Y. Yang, S. Y. Yoon, and I. B. Kang, "An 18 megapixel 4.3″ 1443 ppi 120 Hz OLED display for wide field of view high acuity head mounted displays," J. Soc. Inf. Disp. **26**(5), 314–324 (2018).
5. A. Ghosh, E. P. Donoghue, I. Khayrullin, T. Ali, I. Wacyk, K. Tice, F. Vazan, L. Sziklas, D. Fellowes, and R. Draper, "Directly patterned 2645 ppi full color OLED microdisplay for head mounted wearables," SID Symp. Dig. Tech. Pap. **47**(1), 837–840 (2016).
6. S. Kawashima, H. Shishido, S. Oshita, S. Yoshitomi, A. Yamashita, T. Ishitani, A. Sato, M. Jincho, Y. Shima, M. Katayama, and S. Yamazaki, "A 1058-ppi 4K ultrahigh-resolution and high aperture LCD with transparent pixels using OS/OC technology," SID Symp. Dig. Tech. Pap. **48**(1), 242–245 (2017).
7. H. S. Lee, S. Jang, J. Noh, H. Jeon, B. S. Choi, Y. M. Jeon, K. Song, J. Song, H. Y. Chu, and S. Kim, "An ultra-high density 1.96″ UHD 2250ppi display," SID Symp. Dig. Tech. Pap. **48**(1), 403–405 (2017).
8. K. Kimura, Y. Onoyama, T. Tanaka, N. Toyomura, and H. Kitagawa, "New pixel driving circuit using self-discharging compensation method for high-resolution OLED micro displays on a silicon backplane," J. Soc. Inf. Disp. **25**(3), 167–176 (2017).
9. T. Fujii, C. Kon, Y. Motoyama, K. Shimizu, T. Shimayama, T. Yamazaki, T. Kato, S. Sakai, K. Hashikaki, K. Tanaka, and Y. Nakano, "4032 ppi high-resolution OLED microdisplay," SID Symp. Dig. Tech. Pap. **26**(3), 178–186 (2018).
10. Y. Iwase, A. Tagawa, Y. Takeuchi, T. Watanabe, S. Horiuchi, Y. Asai, K. Yamamoto, T. Daitoh, and T. Matsuo, "A novel low-power gate driver architecture for large 8 K 120 Hz liquid crystal display employing IGZO technology," J. Soc. Inf. Disp. **26**(5), 304–313 (2018).
11. G. Kramida, "Resolving the vergence-accommodation conflict in head-mounted displays," IEEE Trans. Vis. Comput. Graph. **22**(7), 1912–1931 (2016).
12. H. Hua and B. Javidi, "A 3D integral imaging optical see-through head-mounted display," Opt. Express **22**(11), 13484–13491 (2014).
13. Y. H. Lee, G. Tan, T. Zhan, Y. Weng, G. Liu, F. Gou, F. Peng, N. V. Tabiryan, S. Gauza, and S. T. Wu, "Recent progress in Pancharatnam-Berry phase optical elements and the applications for virtual/augmented realities," Opt. Data Process. Storage **3**(1), 79–88 (2017).
14. X. Wang, Y. Qin, H. Hua, Y. H. Lee, and S. T. Wu, "Digitally switchable multi-focal lens using freeform optics," Opt. Express **26**(8), 11007–11017 (2018).
15. Y. Kusakabe, M. Kanazawa, Y. Nojiri, M. Furuya, and M. Yoshimura, "A YC-separation-type projector: High dynamic range with double modulation," J. Soc. Inf. Disp. **16**(2), 383–391 (2008).
16. F. Heide, D. Lanman, D. Reddy, J. Kautz, K. Pulli, and D. Luebke, "Cascaded displays: spatiotemporal superresolution using offset pixel layers," ACM Trans. Graph. **33**(4), 60 (2014).

17. Y. H. Lee, T. Zhan, and S. T. Wu, "Enhancing the resolution of a near-eye display with a Pancharatnam-Berry phase deflector," Opt. Lett. **42**(22), 4732–4735 (2017).
18. J. Y. Wu, P. Y. Chou, K. E. Peng, Y. P. Huang, H. H. Lo, C. C. Chang, and F. M. Chuang, "Resolution enhanced light field near eye display using e-shifting method with birefringent plate," J. Soc. Inf. Disp. **26**(5), 269–279 (2018).
19. T. Zhan, Y. H. Lee, and S. T. Wu, "High-resolution additive light field near-eye display by switchable Pancharatnam-Berry phase lenses," Opt. Express **26**(4), 4863–4872 (2018).
20. G. Osterberg, "Topography of the layer of rods and cones in the human retina," Acta Ophthal. **6**(Suppl.), 1–103 (1935).
21. H. Hua and S. Liu, "Dual-sensor foveated imaging system," Appl. Opt. **47**(3), 317–327 (2008).
22. Y. Qin and H. Hua, "Continuously zoom imaging probe for the multi-resolution foveated laparoscope," Biomed. Opt. Express **7**(4), 1175–1182 (2016).
23. J. P. Rolland, A. Yoshida, L. D. Davis, and J. H. Reif, "High-resolution inset head-mounted display," Appl. Opt. **37**(19), 4183–4193 (1998).
24. M. Shenker, "Optical design criteria for binocular helmet-mounted displays," in Display System Optics, A. Cox, R. Hartmann, eds., Proc. SPIE **778**, 70–78 (1987).
25. U. Konttori, K. Melakari, and O. A. O. Sahlsten, "Display apparatus and method of displaying using focus and context displays," U.S. Patent 9,711,072 (July 18, 2017).
26. K. Akşit, W. Lopes, J. Kim, P. Shirley, and D. Luebke, "Near-eye varifocal augmented reality display using see-through screens," ACM Trans. Graphic **36**(6), 189 (2017).
27. L. Shi, F. C. Huang, W. Lopes, W. Matusik, and D. Luebke, "Near-eye light field holographic rendering with spherical waves for wide field of view interactive 3d computer graphics," ACM Trans. Graphic **36**(6), 236 (2017).
28. A. Bauer, E. M. Schiesser, and J. P. Rolland, "Starting geometry creation and design method for freeform optics," Nat. Commun. **9**(1), 1756 (2018).
29. P. D. Burns, "Slanted-edge MTF for digital camera and scanner analysis," Proc. IS&T 2000 PICS Conference, 135–138 (2000).
30. S. Pancharatnam, "Generalized theory of interference and its applications," Proc. Indian Acad. Sci. A **44**(5), 247–262 (1956).
31. M. V. Berry, "Quantal phase factors accompanying adiabatic changes," Proc. R. Soc. Lond. A **392**(1802), 45–57 (1984).
32. K. Gao, C. McGinty, H. Payson, S. Berry, J. Vornehm, V. Finnemeyer, B. Roberts, and P. Bos, "High-efficiency large-angle Pancharatnam phase deflector based on dual-twist design," Opt. Express **25**(6), 6283–6293 (2017).
33. J. Kim, Y. Li, M. N. Miskiewicz, C. Oh, M. W. Kudenov, and M. J. Escuti, "Fabrication of ideal geometric-phase holograms with arbitrary wavefronts," Optica **2**(11), 958–964 (2015).
34. C. Oh and M. J. Escuti, "Achromatic diffraction from polarization gratings with high efficiency," Opt. Lett. **33**(20), 2287–2289 (2008).

1. Introduction

Recently, head-mounted displays have attracted a great deal of interest due to its potentially wide applications in gaming, education, training and medical care [1,2]. While the visual experience delivered by current augmented reality (AR) and virtual reality (VR) devices is still below what we can perceive in the real world [3]. A significant cause of degraded immersive experience in VR headsets is low resolution. Most of current commercial VR displays can only offer angular resolution of around 10~15 pixel per degree (ppd) in the central region with a FOV ≈110°. However, the acuity of a normal person with 20/20 vision is about 1 arcmin, namely 60 ppd. Thus, the VR headset users can observe clear pixelation and screen-door effect, which would greatly degrade the immersive experience of virtual contents. To eliminate screen-door effect, 4~5 × improvement on angular resolution is needed to match human-eye acuity. However, there exists a trade-off between high angular resolution and wide field of view, as Fig. 1 depicts. In order to obtain ~60 ppd angular resolution while keeping wide FOV >100°, over 6K × 6K pixels would ultimately be needed for each eye. Such a huge increase of display pixel number would inevitably bring new challenges for panel fabrication, driving electronics, image rendering and data transport [3,4]. No matter for liquid crystal display (LCD) or organic light emitting diode (OLED) display, it will be a very challenging task to integrate over 36 million (6K × 6K) pixels on such a small display panel. Thanks to the tremendous efforts of panel manufactures [4–9], the VR display resolution has been pushed to around 4K × 4K recently [4], although there is still a long way to go for low-cost mass production. In addition, the new driving circuitry designs are also required [9,10]

due to the much shorter addressing time for each scan line. Even if such a high-resolution panel can be fabricated and successfully driven, there still exists other issue regarding the display data transport [3,4]. Assuming a 6K × 6K display panel with 90 Hz refresh rate, we need to deliver more than 70 Gb/s to the display, not even to mention light field displays with space- or time-multiplexing [2,11–14]. Due to the limitation from the computing power and data cable bandwidth, more efficient image rendering pipeline must be developed [3]. So far, achieving retina-level resolution near-eye display with wide FOV remains a challenging task. To overcome these issues, several efforts [15–19] have been devoted to enhance the effective resolution by optical methods. For instance, using an image deflector to shift the image by one half of the pixel width to increase the number of pixels has been proposed [17,18]. By doing so, the effective resolution can indeed be doubled except that the required refresh rate is also doubled.
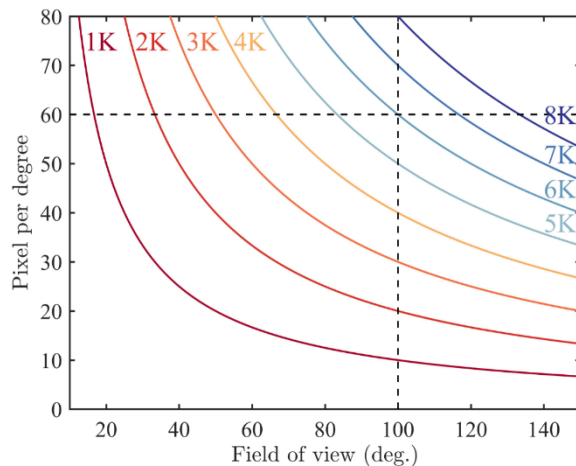

Fig. 1. The trade-off between field of view and angular resolution in near-eye displays for different panel resolutions from 1K to 8K.

As discussed above, simply increasing the pixel number does not seem to be an elegant solution at the current stage. Human visual system should be taken into consideration as well. Actually, our visual system has an efficient information processing architecture. In human retina, the image-capture receptors, namely cone cells, are concentrated in a very narrow central region, called fovea [20]. Therefore, human eye acuity is the highest in the fovea region ($\sim \pm 5°$) and drops rapidly as the eccentricity angle increases. The image acquired by human eye has much higher information content in the fovea region. Such a foveation concept has already been utilized in the imaging system and video processing [21,22]. In terms of VR displays, we only need to provide high resolution for the central fovea region instead of the whole field of view. A foveated display is needed by considering panel fabrication difficulties and data transport issue [23–25]. Several multi-resolution foveated display designs have been proposed [22–24], but these designs are still relatively bulky and difficult to integrate into a compact wearable device. Moreover, such a foveated display should be able to displace high resolution region to enable gaze-contingent technique.

In this paper, we propose a multi-resolution foveated display for near-eye displays. Two display panels are adopted in our system: the first one provides a wide FOV, while the second one offers an ultra-high resolution at the central fovea region. Especially, by an optical minifying system, resolution of the second panel can be enhanced by up to 5 × , which is approaching the human-eye acuity. Moreover, a Pancharatnam-Berry phase deflector (PBD) [13,17] is applied to actively shift the high-resolution region, in order to integrate with gaze-contingent functions. Our proposed design only requires two relatively low-resolution panels, which can avoid the fabrication and driving difficulties for high-resolution display panels. In

addition, the proposed foveated display design can be easily integrated into varifocal light filed display systems [13,14,26,27].
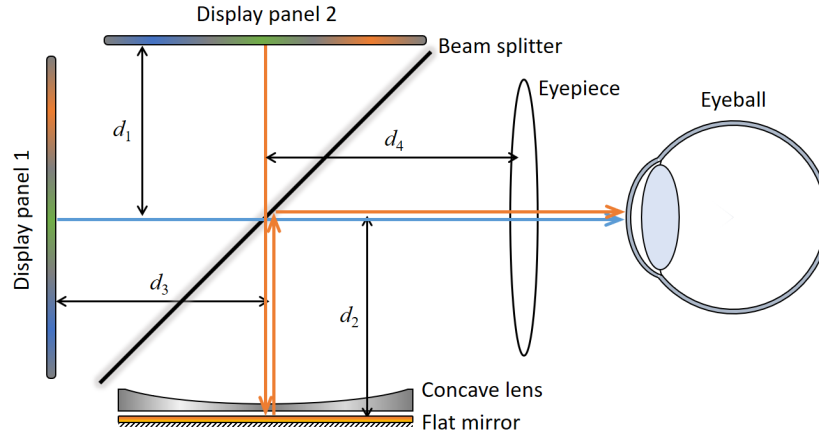
2. System configuration

Fig. 2. Schematic diagram of the proposed multi-resolution foveated display for near-eye display devices.

Figure 2 depicts the system configuration of the proposed multi-resolution display design. Briefly, this design consists of two display panels with a beam splitter (BS) as an optical combiner. The unfolded optics of the proposed design are illustrated in Figs. 3(a) and 3(b). The image displayed by panel 1 will be directly viewed by human eye through beam splitter and eyepiece lens as plotted in Fig. 3(a), which is quite similar to a conventional VR display. However, in our design this display panel only delivers the image content for surrounding region. The light from the second panel will pass through a folded optical path, which includes a concave lens and a flat mirror, as Fig. 2 illustrates. Thus, the image displayed by panel 2 will be minified first by the concave lens [Fig. 3(b)], before it is perceived by human eye. If the focal length of concave lens is denoted as $-f_c$ and the optical minification as M, then the spatial resolution enhancement ratio R can be expressed by:

$$R = \frac{1}{M} = 1 + \frac{d_1 + d_2}{f_c/2},$$

(1)

where $d_1 + d_2$ stands for the distance from display panel 2 to the flat mirror. According to Eq. (1), the enhancement ratio R can be enlarged by reducing the focal length of concave lens or increasing the distance $d_1 + d_2$. Actually, in our following experimental demonstrations, the resolution enhancement can easily reach 4~5x. Therefore, the display 2 can finally generate an ultra-high resolution but small-size image. As mentioned above, two displays provide image contents for central and surrounding regions, respectively. A beam splitter is used to combine these two displayed images together, as shown in Fig. 2. It is worth mentioning that the perceived image depths from two displays must be matched, as Fig. 3(b) illustrates. Thus, the display panel 2 should be placed at:

$$d_3 = d_2 + (d_1 + d_2)/R,$$

(2)

where R is the enhancement ratio from Eq. (1). Then display panel 1 and the virtual image of panel 2 can be located at the same depth [Figs. 3(a) and 3(b)].
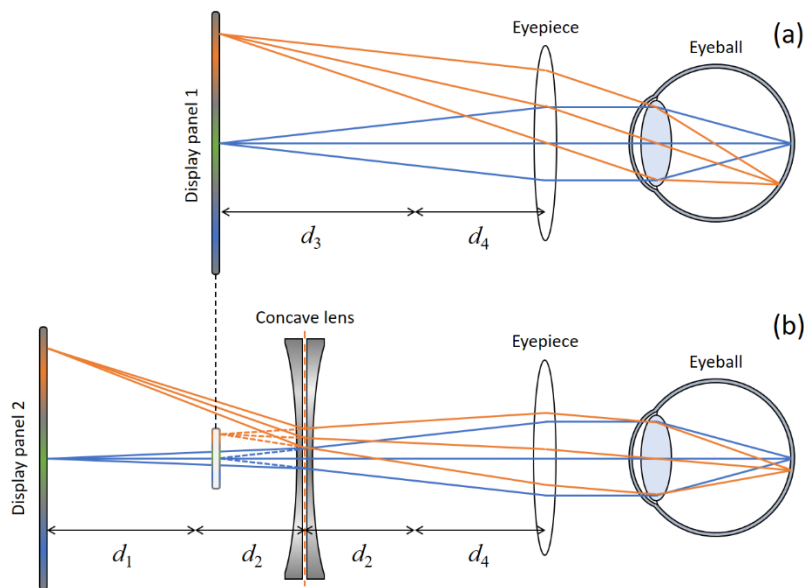
Fig. 3. The unfolded layout of the optical paths for a) display panel 1 and b) panel 2.

3. Experiment

In this section, we carried out experiments to demonstrate our proposed design discussed above. Our optical setup basically followed the layout plotted in Fig. 2. In our experiments, two identical 3.7-inch OLED panels with resolution 1200 × 1080 were employed as the two displays shown in Fig. 2. One plano-concave lens with focus length $-f_c = -35$ mm was adopted. As for the eyepiece, we used a positive achromatic doublet lens with focal length $f_e = 10$ cm in our experiments. Actually, the current VR headset eyepieces, for instance Fresnel lens, can also be used in our design. The angular resolution enhancement ratio will keep the same. The main reason why the achromatic lens with $f_e = 10$ cm is chosen in our experimental setup is to get photography of whole field of view with clear RGB pixels. A camera was placed after the eyepiece lens to capture the displayed images. To eliminate the ghost images generated by panel reflection, we laminated a circular polarizer and an anti-reflection film onto each OLED panel.

In the following experiments, we considered two cases with spatial resolution enhancement ratio $R = 4$ and 5, respectively. According to Eq. (1), we set $d_1 + d_2 \approx 5.25$ cm to achieve around 4 × resolution enhancement and $d_1 + d_2 \approx 7$ cm for 5 × resolution enhancement. For each case, the distance d_3 was adjusted to match the image depths of two displays, as Eq. (2) suggests.

Figures 4 and 5 show the experimental results. The display performance is very good without obvious image distortions. To further minimize the image distortions in future work, the minifying optical path can be improved with multiple lens or freeform lens [28]. As indicated in Figs. 4(a) and 5(a), the displayed image regions enclosed by the black circle have much higher spatial resolution than the outside regions. Especially, from the magnified figures Figs. 4(b) and 5(b), the pixelation or screen-door effect can be observed in the outside low-resolution region. But inside the black circle, images are quite smooth. If we further zoom in the images, the pixel size can be compared directly at the boundary, as depicted in Figs. 4(c) and 5(c). For quantitative evaluations, we first measured the pixel pitch of the OLED panels under an optical microscope, before setting up the foveated display system. Therefore, we are able to measure the pixel pitch in the central and surrounding regions. Then through the photographs, the spatial resolution enhancement ratios can be determined: $R \approx 4$

for Fig. 4 and $R \approx 5$ for Fig. 5. Thus, Fig. 4 and Fig. 5 indicate that we have successfully demonstrated a multi-resolution foveated display using our proposed optical method.
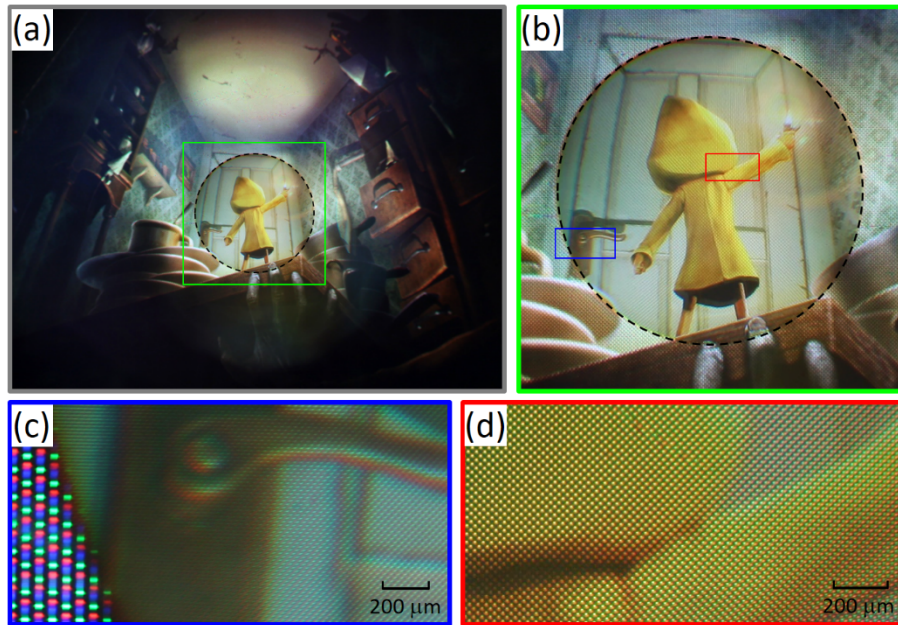

Fig. 4. The experimental photographs with the proposed multi-resolution foveated display with 4 × resolution enhancement: a) displayed image; b) the magnified green square region in (a); c) the magnified blue rectangle region in (b); d) the magnified red rectangle region in (b).
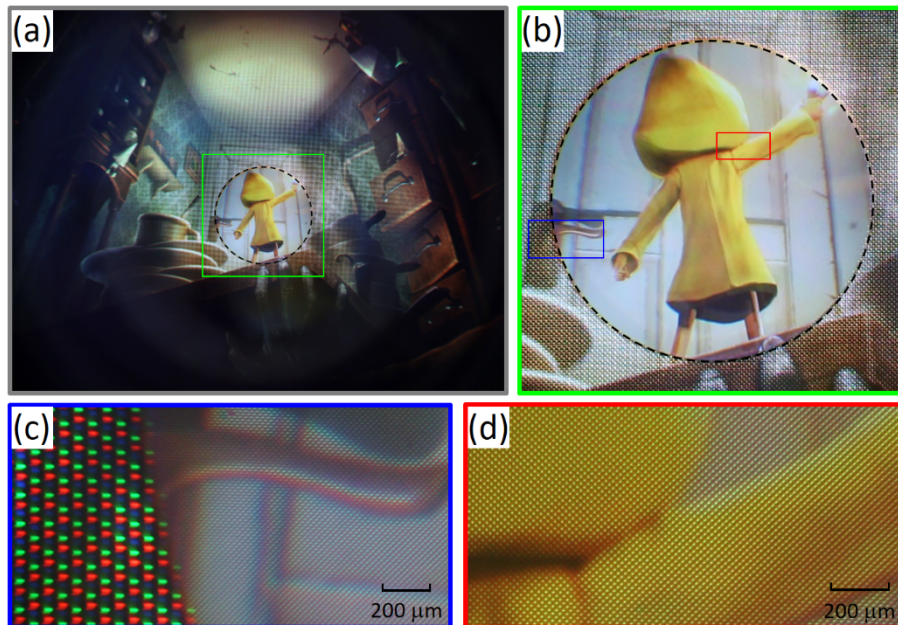

Fig. 5. The experimental photographs with the proposed multi-resolution foveated display with 5 × resolution enhancement: a) displayed image; b) the magnified green square region in (a); c) the magnified blue rectangle region in (b); d) the magnified red rectangle region in (b).

Figures 4 and 5 also illustrate that the spatial resolution enhancement of the central region can be easily tuned by changing $d_1 + d_2$. Higher resolution is achievable, while the trade-off is

the shrunk high-resolution region. By comparing Figs. 4(a) and 5(a), we can clearly see this point. For a commercially available VR display with 1600 × 1440 resolution and 110° horizontal FOV (HTC Vive pro, 2018), it provides angular resolution of around 14.5 ppd. If we apply our 4 × enhancement system, we can obtain ~58 ppd for the central 25° FOV region.

In Fig. 6, we examine the on-axis modulation transfer function (MTF) [29] along two optical paths. The MTF was measured with a Canon EOS T5i camera at F/5.6 with ISO 400 and exposure time 2.5 ms. The MTF of the low-resolution path (Original) drops to 0.5 at 20 cpd, while the high-resolution path (4 ×) drops to 0.5 at 72 cpd. The MTF is not exactly 4 × as high-resolution path involves an extra fast lens, which introduces additional aberration. As the system is operating at 14.5 and 58 ppd for low- and high-resolution images, the imaging performance is reasonably sufficient.
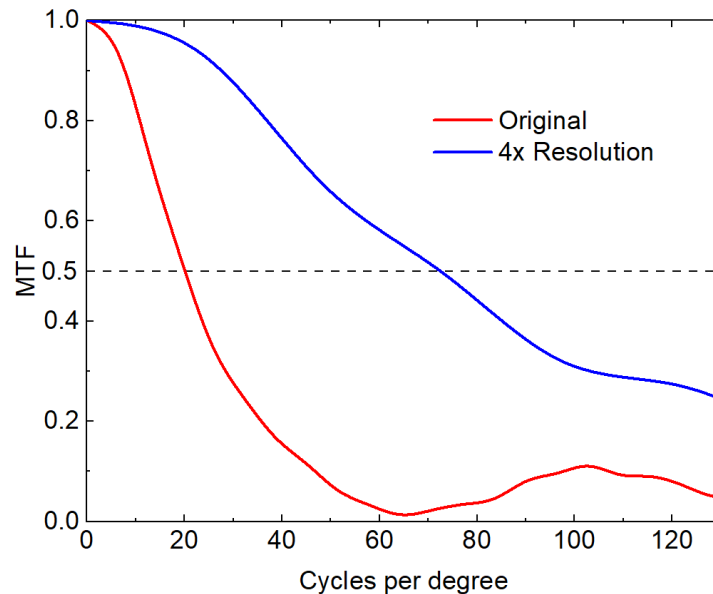

Fig. 6. The measured on-axis modulation transfer function for original and 4 × resolution in angular space. Note that the MTF drops to 0.5 at 20 cpd and 72 cpd for the original and 4 × resolution, respectively.

4. Image shifter

As discussed above, ultra-high angular resolution can be obtained in the narrow central region ~20° FOV. While this region may still not be large enough, since human eye may look at different positions of the display. Eye-gaze tracking techniques need be integrated to provide better viewing experience. To enable eye-tracking function, we propose to use a switchable Pancharatnam-Berry phase deflector (PBD) to shift the high-resolution region and adjust the display contents in real time.

The PBD is a single-order phase grating based on Pancharatnam-Berry phase change [30,31]; in theory its diffraction efficiency can achieve ~100% [13,17,32]. In a PB phase optical element, the half-wave ($\lambda/2$) plate is spatially patterned with varying in-plane crystal axis direction [13]. Its phase modulation is directly determined by the crystal axis orientation, namely liquid crystal azimuthal angle $\varphi(x, y)$. The detailed working mechanism can be explained by Jones matrices. With a circularly polarized input light, the Jones calculus can be written as [17]:

$$J'_{\pm} = R(-\varphi) \cdot W(\pi) \cdot R(\varphi) \cdot \frac{1}{\sqrt{2}} \begin{bmatrix} 1 \\ \pm i \end{bmatrix} = e^{\pm i 2\varphi} \frac{1}{\sqrt{2}} \begin{bmatrix} 1 \\ \mp i \end{bmatrix}, \qquad (3)$$

where J_+ and J_- stand for the left- and right-handed circularly polarized light (LCP and RCP), respectively, $R(\varphi)$ and $R(-\varphi)$ present the rotation operation matrix and $W(\pi)$ is the phase retardation matrix. According to Eq. (3), besides flipping the handedness, the $\lambda/2$ plate also introduces a $\pm 2\varphi(x, y)$ phase delay. If the LC azimuthal angle distribution follows a linear profile as:

$$\varphi(x, y) = (2\pi/P) \cdot x, \qquad (4)$$

then a linear wavefront delay can be constructed, as shown in Fig. 7(a) and 7(b).
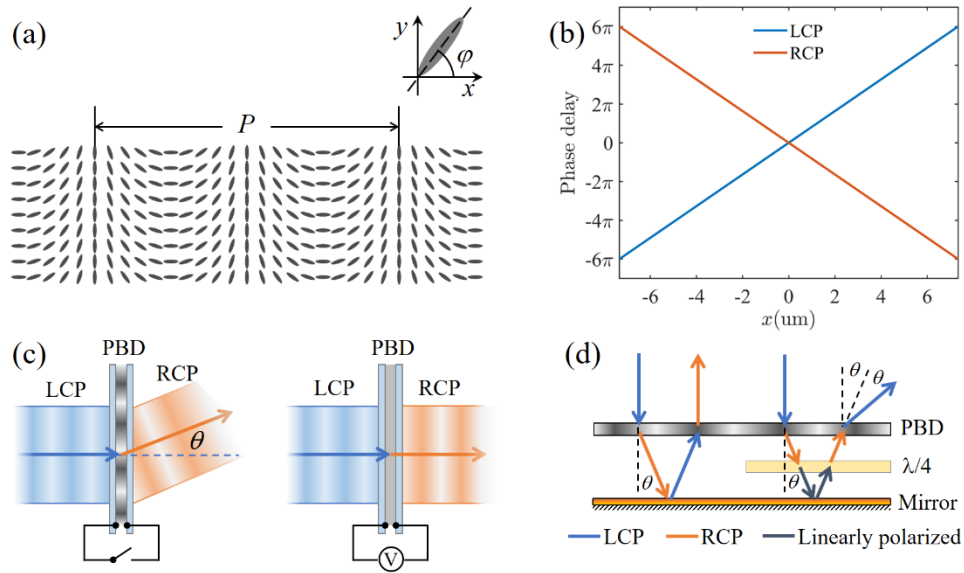

Fig. 7. (a) Top view of the LC director distribution in PBD. (b) Phase delay profile of a PBD with 15° deflect angle at $\lambda = 633$ nm for LCP and RCP, respectively. (c) Active driving to result in a switching between deflection and non-deflection states. (d) The polarization state change for the LCP wave deflected by PBD and reflected by mirror.

Then the PBD can work as a high-efficiency single order phase grating, with the deflection angle [17]:

$$\theta = \arcsin(2\lambda/P). \qquad (5)$$

Detailed theoretical explanations and device fabrication methods can be found in [13,17,32,33]. Both active driving and passive driving schemes can be adopted for driving a PBD [13]. Here we choose the active driving method because PBD will not change the incident light direction at the voltage-on state [Fig. 7(c)].

There are three reasons why we choose a PBD as the image shifter. Firstly, it is a single order deflector with nearly 100% diffraction efficiency, which helps eliminate ghost images. In experiments, over 95% optical efficiency can be easily obtained [13,32,34]. Secondly, the fast switching between two states can greatly reduce the latency for eye-tracking. Both turn-on time and turn-off time of PBD keep shorter than 1 ms [13,17]. The third reason is low operation voltage (7~8 Volts), which helps reduce power consumption.

It is worth mentioning that polarization management needs to be carefully considered for PB optical elements. As plotted in Fig. 7(d), if a PBD is just simply inserted between the

concave lens and the mirror, it works as a simple reflector instead of a deflector because both PBD and metal reflection will flip the polarization handedness. Therefore, we need to add another quarter-wave (λ/4) plate to get the correct polarization state. Finally, the deflection angle of the system combining PBD, λ/4 plate, and mirror is 2θ.
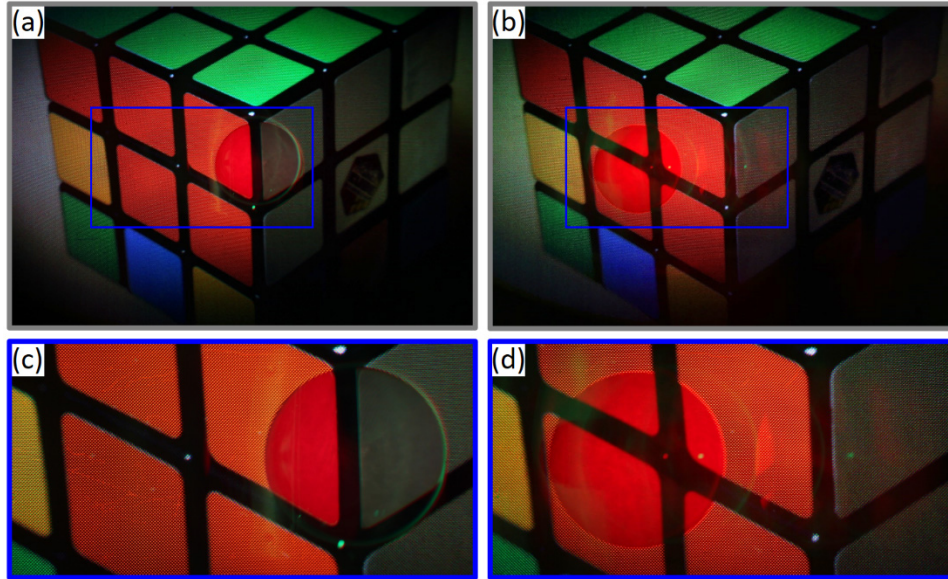

Fig. 8. The experimental results of the proposed multi-resolution display with a PBD as image shifter: a) displayed image with high-resolution region in the center; b) displayed image with shifted high-resolution region; c) the magnified blue rectangle region in (a); d) the magnified blue rectangle region in (b).

To demonstrate this concept by experiments, we inserted a PBD and a broadband quarter-wave plate between concave lens and flat mirror in Fig. 2. The spatial period of the employed PBD is $P = 4.88$ μm, and its deflection angle is 15° for $λ = 633$ nm. The LC birefringence and thickness were carefully tuned to match the half-wave requirement for $λ = 633$ nm. Detailed fabrication procedure of PB elements can be found in [13,17,33]. The above-mentioned OLED panel was still used as display 1. To minimize the possible image blur induced by angular dispersion of diffraction grating, we adopted a 5.5-inch $2560 × 1440$ LCD panel with laser backlight as display panel 2. The three RGB laser wavelengths are $λ_B = 445$ nm, $λ_G = 520$ nm and $λ_R = 639$ nm. A broadband λ/4 plate was also laminated to the LCD panel in order to convert its polarization state to circular polarization. The experimental results are presented in Fig. 8.

From Fig. 8, the high-resolution region is successfully displaced with the help of an image shifting PBD. No obvious image blur occurs since the diffraction efficiency of PBD is over 95%. The preliminary results shown in Fig. 8 serve the purpose as feasibility demonstration. In reality, the deflection angles of the three laser wavelengths are different, due to the angular dispersion of diffraction gratings. That would lead to color breakup in the shifted high-resolution region. To overcome this issue, pre-compensation should be carried out when processing display images from panel 2.

5. Conclusion

We have experimentally demonstrated a multi-resolution foveated display for VR applications. The proposed design mainly consists of two display panels and an optical combiner. We used the first display to provide a wide FOV and the second display to offer an ultra-high resolution for the central fovea region. The spatial resolution of the second display

is enhanced by 5 × , by an optical minifying system. In addition, an image shifter PBD is also employed to relocate the high-resolution region. The proposed optical system can effectively reduce the screen-door effect in near-eye displays.